Appendix S1.
Summary Geological Map of NE Iran

Figure S1 below shows a summary geological map of the major units in the NE Iran region, simplified from the 1:2,500,000 scale map of the National Iranian Oil Company (1957). Although more comprehensive geological maps for this region are available from the Geological Survey of Iran (see Fig. S1 caption), this figure is provided as a simple reference map for the areas discussed in the main paper.

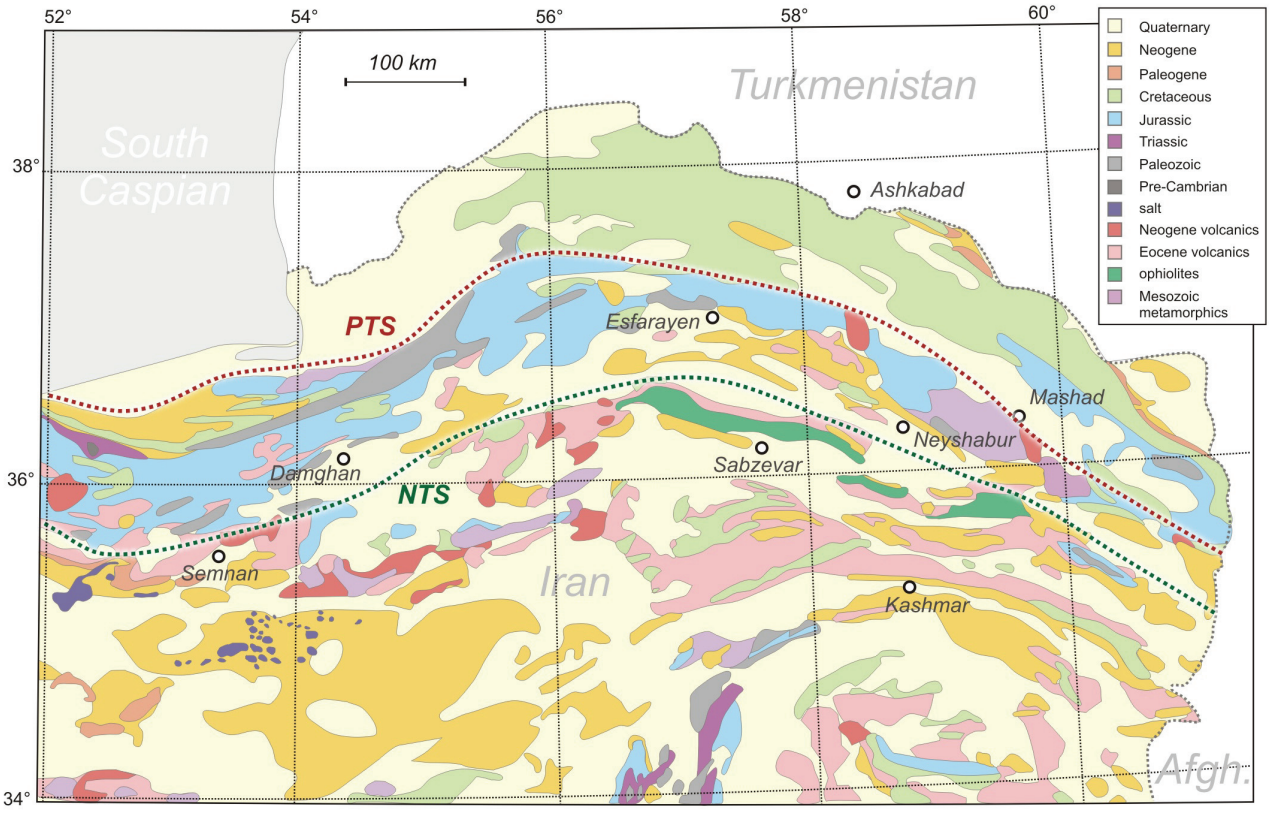

Figure S1. Simplified geological map showing the major units throughout the NE Iran region (based on the National Iranian Oil Company, 1957). For further resources on the geology of Iran and to download more recent and detailed geological maps, visit the website of the Geological Survey of Iran (GSI) at www.gsi.ir/Product/ Lang_en/Page_38/index.html, and see also the USGS open file report of Pollastro, et al. (1997). Dashed red and green lines show the approximate locations of the Paleotethys and Neotethys Suture Zones (see Section 2.2 for details). Ophiolitic material associated with the Neotethys Suture Zone lies north of Sabzevar and Kashmar.

References

Fattahi, M., Walker, R., Hollingsworth, J., Bahroudi, A., Nazari, H., Talebian, M., Armitage, S., & Stokes, S., 2006. Holocene slip-rate on the Sabzevar thrust fault, NE Iran, determined using optically stimulated luminescence (OSL), *Earth and Planetary Science Letters*, 245(3–4), 673–684.

National Iranian Oil Company (NIOC), 1957. Geological Map of Iran (1:2,500,000).

Pollastro, R. M., Persits, F., & Steinshouer, D., 1997. Map showing geology, oil and gas fields, and geological provinces of Iran, *USGS Open-File Report 97–470G*, http://pubs.usgs.gov/of/1997/ofr–97–470/OF97–470G/.

Appendix S2.
Optically Stimulated Dating methodology for the Neyshabur and North Neyshabur faults

Optically stimulated luminescence (OSL) dating measures the time since quartz-rich sedimentary material was last exposed to sunlight. If sediment deposition is relatively continuous, such as from an active alluvial fan at the edge of a mountain range, the time since the material was last exposed to sunlight is thought to represent the age of deposition. If a once continuous abandoned alluvial fan becomes gradually displaced across an active fault during a number of earthquake cycles, both the age of the fan surface and the amount of displacement can be used to determine the rate of slip on the fault. Knowledge of fault slip rates is paramount to our understanding of how regions actively deform. Furthermore, if the repeat time for earthquakes can be determined, either from length-scaling relationships or detailed paleoseismology studies, the seismic hazard posed to nearby population centres can be established.

Upon deposition of quartz-rich sediments, low-level background radiation causes free electrons within the quartz crystal lattice to be excited from the lower energy valence band to the higher energy conduction band. Some of these electrons become `trapped' metastably between the two energy levels in defects within the crystal lattice. The longer these sediments are buried, the more electrons accumulate in traps. Small amounts of energy, such as sunlight, cause `trapped' electrons to return to their lower energy valence band, releasing photons in the process. This can be measured in the laboratory as a luminescence signal, when the sample is exposed to a light source. The degree of luminescence is thought to be equivalent to the total amount of radiation the sediments have been exposed to since burial (known as equivalent dose, or paleodose, D_e). The age of deposition is calculated from the paleodose and the present-day rate of background radiation at the sample site (dose rate, D_r – measured using a gamma ray spectrometer). Typically, each sample is divided into a number of aliquots and the paleodose is measured for each one. If the spread of paleodose measurements is low, the average paleodose between all aliquots is used in the age calculation. If there is a large spread in paleodose between aliquots, the sample may not have been exposed to enough sunlight required to reset all the trapped electrons prior to deposition. In this case, the smallest paleodose (equivalent to the youngest age) is thought to represent the time of deposition, and all higher paleodose measurements are the result of grains which have not been fully reset. All samples were analysed on a Riso (Model TL/OSL-DA-15) automated TL/OSL system under subdued red light. A detailed account of the method used is given in Fattahi & Walker (2007), with further examples of this technique being applied across NE Iran in Fattahi, et al. (2006) and Fattahi, et al. (2007).

References

Fattahi, M., Walker, R., Hollingsworth, J., Bahroudi, A., Nazari, H., Talebian, M., Armitage, S., & Stokes, S., 2006. Holocene slip-rate on the Sabzevar thrust fault, NE Iran, determined using optically stimulated luminescence (OSL), *Earth and Planetary Science Letters*, 245(3–4), 673–684.

Fattahi, M. & Walker, R., 2007. Luminescence dating of the last earthquake of the Sabzevar thrust fault, NE Iran, *Quaternary Geochronology*, 2, 284–289.

Fattahi, M., Walker, R., Khatib, M., Dolati, A., & Bahroudi, A., 2007. Slip-rate estimate and past earthquakes on the Doruneh fault, eastern Iran, *Geophysical Journal International*, 168, 691–709.

Appendix S3.
Determining horizontal shortening rates

The contribution of the North Neyshabur fault to regional shortening may be determined in two ways, depending on the structure of the fault with depth (Fig. S3). If the fault dips north at 60° and cuts the entire crust, the fault slip rate (z) may be resolved onto its vertical uplift (y) and horizontal shortening (x) components (Fig.S3a and b). In the case of the North Neyshabur fault, this would yield a shortening rate of 0.3–0.5 mm/yr (see Table 2 of the main paper). However, if the fault shallows with depth onto a horizontal décollement, commonly seen in active thrust systems bounding mountain ranges (e.g. Tien Shan, Daeron, et al., 2007; Himalaya and Tibet, Meyer, et al., 1998, and Lavé J. & Avouac, 2000; and Taiwan, Simoes, et al., 2007) then the shortening rate on the décollement will equal the fault slip rate (z) where the fault ramps to the surface (Fig.S3c and d). In this case, the shortening rate across the North Neyshabur fault will be slightly higher (0.7–1.0 mm/yr) than the rate determined by resolving fault slip onto its vertical and horizontal components (see Table 2 of the main paper). To determine which shortening rate estimate is correct for the North Neyshabur fault knowledge is required of the subsurface structure across the fault, which may be revealed by seismic reflection experiments. As we lack this information, our estimate for the shortening rate across this fault incorporates both rates estimated above as upper and lower bounds, yielding 0.3–1.0 mm/yr.

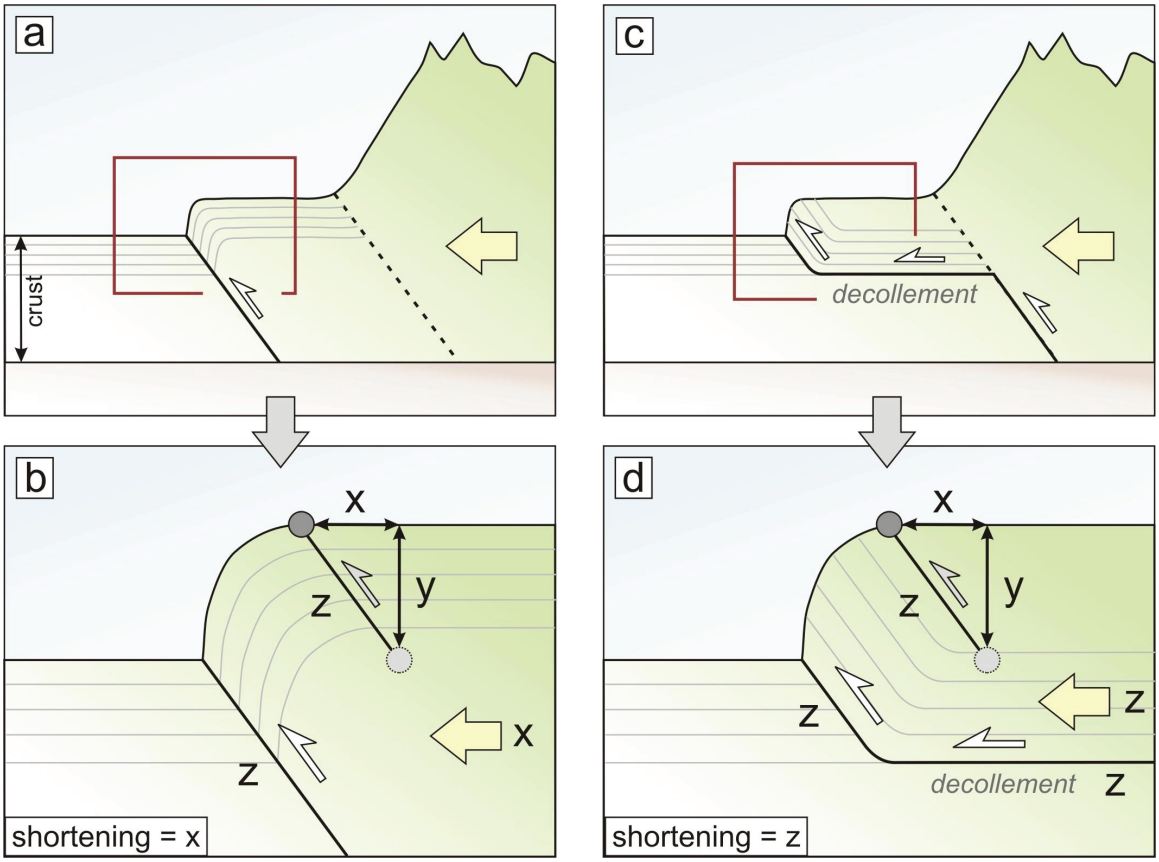

Figure S3. (a) Schematic geological cross-section in which horizontal shortening across a mountain range (yellow arrow) is accommodated by slip on a range bounding single planar thrust fault which cuts the entire crust at an angle of 60°. Faulting has stepped basinward of the mountains and the older range bounding thrust (shown by a dashed black line) is relatively inactive. Where the younger and more active thrust fault comes to the surface (shown by the red box), the youngest sedimentary deposits (grey lines) are offset vertically, producing a step, shown in (b). Because the regional shortening is accommodated by movement on a dipping fault which cuts the entire brittle crust, the slip on the fault plane (z) is resolved onto a horizontal (x) and vertical (y) component. The rate of uplift, which only records the vertical component of motion over time, may be determined if both the age of the displaced surface deposits, and the amount of vertical displacement are known. However, to determine the horizontal component of shortening, knowledge of the fault plane geometry is required to determine both the fault slip-rate (z) and the horizontal shortening rate (x). The typical motion of the surface deposits before and after a period of movement on the fault is indicated by the light grey circle (pre-fault movement), and the dark grey circle (post-fault movement). In this model, the shortening rate (x) will always be less than the fault slip-rate (z). (c) Geological cross section across a mountain range in which shortening is accommodated by slip on a dipping thrust fault at depth, and slip on a horizontal décollement at shallower depths which ramps to the surface away from the range front. (d) In this model, material in the hanging wall above the décollement is extruded at the rate z everywhere along the basal thrust. The structure of the deformed geology across the fault zone is significantly different from that shown in (b), allowing the differentiation between these two models by field observations of dipping strata. The typical motion of deformed surface deposits before and after a period of shortening is shown by the light and grey circles. In this model, the horizontal component of motion will decrease locally to x where the décollement ramps to the surface. However, away from the ramp the regional horizontal shortening rate is given by the higher value of z (which in turn must be the horizontal component of shortening across the dipping thrust fault at depth).

References

Daëron, M., Avouac, J.-P., & Charreau, J., 2007. Modeling the shortening history of a fault-tip fold using structural and geomorphic records of deformation, *Journal of Geophysical Research*, 112, B03S13.

Lavé J., & Avouac, J.-P., 2000. Active folding of fluvial terraces across the Siwalik Hills (Himalaya of central Nepal), *Journal of Geophysical Research*, 105, 5735–5770.

Meyer, B., Tapponnier, P., Bourjot, L., M´etivier, F., Gaudemer, Y., Peltzer, G., Shunmin, G., & Zhitai, C. (1998). Crustal thickening in Gansu-Qinghai, lithospheric mantle subduction, and oblique, strike-slip controlled growth of the Tibet plateau. *Geophysical Journal International*, 135(1), 1–47.

Simoes, M., Avouac, J.-P., Chen, Y.-G., Singhvi, A., Wang, C.-Y., Jaiswal, M., Chan, Y.-C., & Bernard, S., 2007. Kinematic analysis of the Pakuashan fault tip fold, west central Taiwan: Shortening rate and age of folding inception, *Journal of Geophysical Research*, 112, B03S14.

Appendix S4.
Elastic dislocation modelling of the Neyshabur fault

An estimate of the Neyshabur fault geometry is obtained using an elastic dislocation model to reproduce the topography created by slip on the fault, following the approach of King, et al., 1988 and Stein, et al., 1988; see Fig.S4. Although this approach does not account for topography created by interseismic deformation, the small <5 km wavelength of this fold compared with the higher >10 km wavelength of flexural deformation produced by gravity, erosion and sedimentation means we can ignore these effects over geological timescales (Benedetti, et al., 2000). Furthermore, we do not account for any postseismic deformation, which we assume is small relative to the coseismic signal (e.g. inclusion of the postseismic signal made only a small contribution to the total deformation for the 365AD earthquake in the Eastern Mediterranean, Shaw, et al., 2008). In our model, fault parameters are varied to produce a pattern of surface deformation which best fits a topographic profile across the fault.

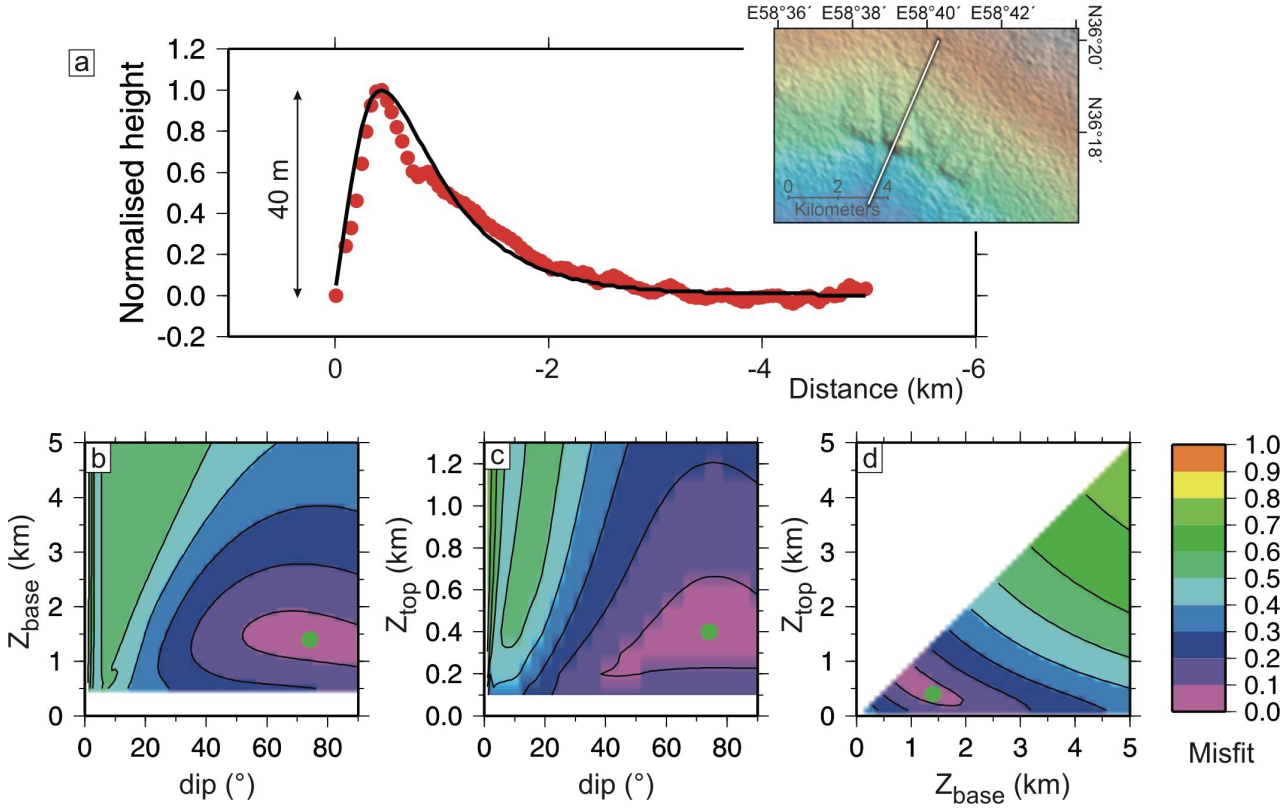

Figure S4. (a) The likely fault parameters for the Neyshabur fault near Shori are determined using elastic dislocation modelling. Red dots show elevations extracted from SRTM data across the fault, which are normalized to values between 0 and 1 and have the regional slope removed (see inset for profile location). Different fault parameters are used to generate the topography resulting from a dislocation in an elastic half space (Okada, 1985), which best fits a normalized topographic profile across the fault. The black line shows the best-fitting model solution, which corresponds to a fault dipping north at 75°, and extending between 0.3–1.5 km depth. Plots (b-d) show the misfit and trade-off between different fault parameters (green is high misfit, purple is low misfit). Depth to the bottom of the faulting is given by Z_{base}, depth to the top of the faulting is Z_{top}, and dip is fault dip in degrees. The broad minimum in each case shows the fault parameters are poorly constrained (i.e. a large trade-off exists between the different parameters). Nevertheless, the dip is likely to be high (50–80°), and the depth to top of faulting (0.5 km) and depth to bottom (1 km) suggest slip occurs on a blind thrust ramp which splays out from the North Neyshabur fault to the north. We use a dip of 60° to calculate fault slip and shortening rates across this fault segment (see Table 3). Although this is a relatively high angle for a thrust fault, a similar dip was measured in the field along the North Neyshabur fault (Section 3.1) and Sabzevar faults (Fattahi, et al., 2006).

References

Benedetti, L., Tapponnier, P., King, G., Meyer, B., & Manighetti, I., 2000. Growth folding and active thrusting in the Montello region, northern Italy, *Journal of Geophysical Research*, 105, 739–766.

Fattahi, M., Walker, R., Hollingsworth, J., Bahroudi, A., Nazari, H., Talebian, M., Armitage, S., & Stokes, S., 2006. Holocene slip-rate on the Sabzevar thrust fault, NE Iran, determined using optically stimulated luminescence (OSL), *Earth and Planetary Science Letters*, 245(3–4), 673–684.

King, G., Stein, R., & Rundle, J., 1988. The growth of geological structures by repeated earthquakes, 1: Conceptual framework, *Journal of Geophysical Research*, 93, 13307–13318.

Okada, Y., 1985. Surface deformations due to shear and tensile faults in a half-space, *Bulletin of the Seismological Society of Americ*a, 75, 1135–1154.

Shaw, B., Ambraseys, N., England, P., Floyd, M., Gorman, G., Higham, T., Jackson, J., Nocquet, J.-M., Pain, C., & Piggott, M., 2008. Eastern Mediterranean tectonics and tsunami hazard inferred from the AD 365 earthquake, *Nature Geoscience*, 1, 268–276.

Stein, R., King, G., & Rundle, J., 1988. The growth of geological structures by repeated earthquakes, 2: Field examples of continental dip-slip faults, *Journal of Geohysical Research*, 93, 13319–13331.